Solution-Phase Grafting of Titanium Dioxide onto the Pore Surface of Mesoporous Silicates: Synthesis and Structural Characterization

Blake J. Aronson, Christopher F. Blanford, and Andreas Stein*

Department of Chemistry, University of Minnesota, 207 Pleasant St. SE, Minneapolis, Minnesota 55455

Received March 31, 1997. Revised Manuscript Received August 27, 1997[⊗]

Titanium dioxide, a large-bandgap semiconductor and versatile photocatalyst, has been grafted onto the pore surface of MCM-41 and FSM-16 (a mesoporous material derived from kanemite) by reacting $TiCl_4$ in hexanes with the as-synthesized mesostructured silicate. The products have been extensively characterized by powder XRD, TEM, SEM, EDS, XPS, N_2 adsorption, SANS contrast matching, solid-state ^1H MAS NMR, IR, and UV−vis spectroscopies. It was found that titania forms well-dispersed isolated $(TiO_2)_n$ clusters ($n \sim 30-70$) within the channel structure. These are attached to the silicate walls via Si−O−Ti bonds. A minor second phase consisting of anatase crystallites ca. 100−250 Å in diameter on the external surface of the mesoporous silicate crystals was sometimes obtained. It is concluded that an organic moiety, such as the surfactant present in the pores, or a physical constraint, such as the pore walls, is necessary to prevent the creation of large TiO_2 agglomerates and enable the formation of nanosized TiO_2 clusters. The titania-grafted MCM-41 samples exhibited good catalytic activity for photobleaching of rhodamine-6G and for oxidation of α-terpineol; however, product selectivity was low.

Introduction

Mesoporous silicates, such as MCM-41,[1] produced from the cooperative self-assembly interaction of a surfactant and a silica source, have been a subject of great interest.[2−7] MCM-41 and similarly synthesized mesoporous materials[8] possess high surface areas, ordered frameworks, and narrow pore size distributions, giving them potential applications as chromatographic materials, host structures, and catalysts for reactions involving large molecules.[9] To effect such applications, however, the pore surface must be modified. Several reports have described the addition of metal oxide centers to mesoporous silica by grafting titanium dioxide, manganese oxide, and vanadium oxide onto the pore surfaces using the organometallic precursors titanocene dichloride,[10] manganese decacarbonyl,[11] and vanadium tetrakisisopropoxide.[12] For each of these systems an organometallic precursor was reacted with a calcined sample of the mesoporous silicate, resulting in isolated centers of the surface species. $TiCl_4$ has been avoided as the titania source because of its tendency to polymerize uncontrollably and form large titania agglomerates rapidly. This paper describes the grafting of $TiCl_4$ onto the pore surface of mesoporous materials by a new method that avoids pore clogging. Under appropriate conditions this controlled modification of the pore surface with titania stabilizes the hexagonal wall structure and permits size quantization of the titania on the high surface area support.

Titanium dioxide is well-known as a large-bandgap semiconductor and versatile photocatalyst. It has been shown to catalyze the splitting of water,[13] as well as many selective oxidation reactions, such as the conversion of ethanol to acetaldehyde[14] and the epoxidation of 1-hexene.[15] Titania can also be used as a catalyst for the synthesis of peptide oligomers from methane and ammonia and the reduction of some organic molecules, such as the methylviologen cation.[14] However, titania is most actively studied for its ability to catalyze the complete degradation of many organic contaminants and environmental toxins. The titania-catalyzed total oxidation reactions of aliphatic and aromatic alcohols as well as organic chlorides to CO_2, H_2O, and HCl have

[⊗] Abstract published in *Advance ACS Abstracts,* October 15, 1997.

(1) Beck, J. S.; Vartuli, J. C.; Roth, W. J.; Leonowicz, M. E.; Kresge, C. T. *J. Am. Chem. Soc.* **1992**, *114*, 10834.
(2) Chen, C. Y.; Li, H. X.; Davis, M. E. *Micropor. Mater.* **1993**, *2*, 17.
(3) Luan, Z.; Cheng, C. F.; Zhou, W.; Klinowski, J. *J. Phys. Chem.* **1995**, *99*, 1018.
(4) Kim, J. M.; Kwak, J. H.; Jun, S.; Ryoo, R. *J. Phys. Chem.* **1995**, *99*, 16742.
(5) Beck, J. S.; Vartuli, J. C.; Kennedy, G. J.; Kresge, C. T.; Roth, W. J.; Schramm, S. E. *Chem. Mater.* **1994**, *6*, 1816.
(6) Huo, Q.; Margolese, D. I.; Stucky, G. D. *Chem. Mater.* **1996**, *8*, 1147.
(7) Wu, C. G.; Bein, T. *Chem. Commun.* **1996**, 925.
(8) Mesoporous refers to pore diameters in the range, 20−500 Å. Sing, K. S. W.; Everett, D. H.; Haul, R. A. W.; Moscou, L.; Pierotti, R. A.; Rouquérol, J.; Siemieniewska, T. *Pure Appl. Chem.* **1985**, *57*, 603.
(9) Chenite, A.; Page, Y. L. *Chem. Mater.* **1995**, *7*, 1015.
(10) a) Maschmeyer, T.; Rey, F.; Sankar, G.; Thomas, J. M. *Nature* **1995**, *378*, 159. b) Walker, J. V.; Morey, M.; Carlsson, H.; Davidson, A.; Stucky, G. D.; Butler, A. *J. Am. Chem. Soc.* **1997**, *119*, 6921−6922.
(11) Burch, R.; Cruise, N.; Gleeson, D.; Tsang, S. C. *Chem. Commun.* **1996**, 951.
(12) Morey, M.; Davidson, A.; Eckert, H.; Stucky, G. D. *Chem. Mater.* **1996**, *8*, 486.
(13) Linsebigler, A. L.; Lu, G.; J. T. Yates, J. *Chem. Rev. (Washington, D.C.)* **1995**, *95*, 735.
(14) Fox, M. A.; Dulay, M. T. *Chem. Rev. (Washington, D.C.)* **1993**, *93*, 341.
(15) Blasco, T.; Corma, A.; Navarro, M. T.; Pérez-Pariente, J. *J. Catal.* **1995**, *156*, 65.

S0897-4756(97)00180-4 CCC: $14.00

been explored.[16−18] Because of its nontoxicity and its ability to destroy organic contaminants, UV-irradiated titania has recently been investigated as a potential disinfectant for small drinking water systems.[19]

Incorporation of titania into various amorphous and zeolitic supports has been studied extensively.[20−23] Such research is of interest for several reasons. First, grafting of a catalytic material onto a support of high surface area (>200 m^2/g) increases the active surface area of the catalyst, often making it more effective. Further, by varying the pore geometry of the support, the catalyst can become size and shape selective. Finally, it is known that the photocatalytic characteristics are often enhanced by quantum size effects for nanometer-sized semiconductor particles.[24] Narrow size distributions for quantum size particles can be attained by confining the particles inside an ordered host material.[25]

The present paper details the results of using a new technique for the grafting of titania onto the pore surface of MCM-41. $TiCl_4$ was reacted with as-synthesized samples of MCM-41 and FSM-16. Clogging of channels with titania was avoided by introducing the reagent when surfactant was still present in the mesopores. Additionally, because calcination results in removal of hydroxyl sites through further SiO_2 condensation, the as-synthesized material had a greater number of reactive silicon hydroxide sites available for titania anchoring. The samples were then exposed to air to hydrolyze the $TiCl_4$ to TiO_2 and calcined to remove the surfactant. The products were extensively characterized by powder XRD, TEM, SEM, EDS, XPS, N_2 adsorption, SANS contrast matching, solid-state ^1H MAS NMR, IR, and UV−vis spectroscopies. The combined data demonstrate that well-dispersed, isolated titania nanoclusters (∼30−70 Ti atoms per cluster) were attached to the silicate walls via Si−O−Ti bonds, and that a significant fraction of them was present on the internal surface of the mesoporous sieves. High surface areas were maintained, and the thermal stability of the framework was increased.

Experimental Section

Materials. Reagents were obtained from the following sources: N brand sodium silicate, PQ Corp.; Ultrasil VN 3SP, P25 titania (70:30 anatase:rutile, nonporous, BET surface area 55 m^2/g, average particle size 30 nm), Degussa Corp.; cetyltrimethylammonium bromide (CTAB), dodecyltrimethylammonium bromide (DTAB), titanium tetrachloride, hexanes, Aldrich; cetyltrimethylammonium chloride (CTACl), TCI; acetone, Mallinckrodt. The D_2O used in the SANS density matching experiments was obtained from Aldrich. The hexanes and acetone were dried over molecular sieves prior to use; otherwise the chemicals were used without further purification.

Technique. The supports used were MCM-41 and FSM-16, a mesoporous material made from kanemite. They were prepared with CTAB or CTACl, respectively, according to literature techniques.[5,26,27] A small amount of the product was set aside and calcined by slow heating to 550 °C under flowing nitrogen, then at 550 °C for 10 h under flowing air. This ungrafted portion was analyzed along with its Ti-grafted counterpart for accurate comparison of the results. Before each sample was grafted, the as-synthesized white powder was dried (i.e., with the surfactant intact) under vacuum at 250 °C for a minimum of 15 h. It was cooled to room temperature, and a slightly pale yellow solution of $TiCl_4$ in hexanes was added under nitrogen (pure $TiCl_4$ is naturally pale yellow). Approximately 0.1 mL of $TiCl_4$/1 g of support was used. The sample became bright yellow upon addition of the $TiCl_4$ solution. It was stirred under nitrogen at room temperature for 4−24 h. The sample was washed with hexanes under nitrogen several times, and the excess solvent evaporated under vacuum overnight at room temperature. Hydrolysis and condensation of the $TiCl_4$ to TiO_2 and removal of the surfactant were carried out simultaneously via calcination as described above. During the product transfer to the calcination oven, which was performed in an open atmosphere, the yellow color began to fade, indicating hydrolysis of the $TiCl_4$ to TiO_2. However, the color faded at a rate substantially slower than the nearly instantaneous hydrolysis of pure $TiCl_4$.

The grafting of a second dose of titania was accomplished by one of two methods. In the first technique, a singly grafted sample was dispersed in an aqueous solution of DTAB for 24 h, followed by rinsing in water and air-drying. The surfactant exposure was repeated once more before the sample was dried and exposed to $TiCl_4$ as outlined above. Alternatively, the second grafting of titania was accomplished by drying of the calcined singly grafted sample under vacuum overnight at 250 °C, followed by a 24-hour exposure of the sample to a bright red solution of $TiCl_4$ in dried acetone. The sample was rinsed with acetone, the solvent evaporated under vacuum, and the sample calcined as described earlier. A comparative experiment was performed on nonporous silica by combining CTAB and Ultrasil in an approximate 3:1 mass ratio, drying under vacuum, and treating with $TiCl_4$ as for the mesoporous systems. A bulk TiO_2 sample was prepared by dissolving $TiCl_4$ in hexanes and allowing the solvent to evaporate in air. The amorphous titania resulting from this procedure was calcined as described above. The product, consisting of ca. 1−10 μm particles, was confirmed to be anatase by powder XRD.

Equipment and Analysis. Powder XRD patterns were collected on a Siemens D-500 wide-angle diffractometer with Cu Kα radiation. Transmission electron microscopy (TEM) was carried out on a Philips CM30 transmission electron microscope operated at 300 kV with a LaB_6 filament. Images were recorded on film. Samples were prepared by mixing the powder with absolute ethanol and sonicating for at least 30 min. The suspension was dripped on a holey carbon grid (Ted Pella, Inc.) and allowed to dry. X-ray energy-dispersive spectra (EDS) were obtained from an attached EDAX PV9900 energy-dispersive spectrometer equipped with an ultrathin window detector and operating with a resolution of 165 eV. X-ray elemental mapping was performed on a JEOL 840 SEM using NIH Image 1.60 and DTSA 2.0.1 to analyze the raw data. Elemental analysis was carried out by the University of Minnesota Geochemical Lab. IR spectra were taken on a Perkin-Elmer 1600 Series FTIR, with a resolution of 4 cm^{-1}. XPS analysis was performed at the University of Minnesota Surface Analysis Center using a Physical Electronics PHI5400 X-ray photoelectron spectrophotometer with a Mg anode (1253.6 eV) operating at 300 W. Charging effects were corrected by adjusting the C_{1s} peak to 284.6 eV. Spectra of Si

(16) Matthews, R. W.; McEvoy, S. R. *J. Photochem. Photobiol. A: Chem.* **1992**, *64*, 231.
(17) Muneer, M.; Das, S.; Manilal, V. B.; Daridas, A. *J. Photochem. Photobiol. A: Chem.* **1992**, *63*, 107.
(18) Ollis, D. F.; Hsiao, C. Y.; Budiman, L.; Lee, C. L. *J. Catal.* **1984**, *88*, 89.
(19) Richardson, S. D.; Thruston, A. D.; Collette, T. W.; Patterson, K. S.; Lykins, B. W.; Ireland, J. C. *Environ. Sci. Technol.* **1996**, *30*, 3327.
(20) Anpo, M.; Aikawa, N.; Kubokawa, Y.; Che, M.; Louis, C.; Gamello, E. *J. Phys. Chem.* **1985**, *89*, 5017.
(21) Reddy, J. S.; Sayari, A. *J. Chem. Soc., Chem. Commun.* **1995**, 23.
(22) Perego, G.; Bellussi, G.; Corno, C.; Taramasso, M.; Buonomo, F.; Eposito, A. *New Developments in Zeolite Science and Technology, Proceedings of the Seventh International Zeolite Conference, Tokyo*, **1984**, 129.
(23) Gontier, S.; Tuel, A. *Zeolites* **1995**, *15*, 601.
(24) Anpo, M.; Shima, T.; Kodama, S.; Kubokawa, Y. *J. Phys. Chem.* **1987**, *91*, 4305.
(25) Ozin, G. A. *Adv. Mater.* **1992**, *4*, 612−649.
(26) Chen, C. Y.; Xiao, S. Q.; Davis, M. E. *Micropor. Mater.* **1995**, *4*, 1.
(27) Beneke, K.; Lagly, G. *Am. Miner.* **1977**, *62*, 763.

2p, O 1s, Ti $2p_{3/2}$, and Ti $2p_{1/2}$ were recorded. Sensitivity factors supplied with the instrument were employed to calculate the atomic ratios. Peaks were deconvoluted using Physical Electronics Software Model 8503A, Version 3.0B. Ti $2p_{3/2}$ and Ti $2p_{1/2}$ peaks were coupled for the deconvolution process.

Diffuse UV−vis spectra were taken on the Hewlett-Packard 8254A diode array spectrophotometer with a Labsphere RSA-HP-84 reflectance spectroscopy accessory; the instrument has a resolution of 2 nm. Reflectance data were converted to $f(R_\infty)$ values, which are directly proportional to absorbance, using the Kubelka−Munk equation. The band edge of the samples was determined by performing a linear regression on the appropriate section of the spectrum using the Microsoft Excel spreadsheet program; to ensure precision in the measurements, several spectra were taken and analyzed for each sample. N_2 adsorption experiments were performed on the Micromeritics ASAP 2000 accelerated surface area and porosimetry system. Small-angle neutron-scattering (SANS) experiments were performed at the SAND beamline of the Intense Pulsed Neutron Source (IPNS) at Argonne National Labs, Argonne, IL. Samples were loaded into a Suprasil cylindrical cell with a 1 mm path length. The scattered neutrons were measured using a 128 × 128 array of position sensitive, gas filled, 40 × 40 cm^2, proportional counters with the wavelengths measured by time-of-flight with data in the Q range of 0.0035−0.8 $Å^{-1}$ taken in a single measurement.

Catalytic Testing. *Rhodamine-6G Photodegradation.* Prior to the reaction, the catalyst samples were either irradiated overnight to remove any residual organic matter or stirred in a 1.00 mM aqueous solution of rhodamine-6G (Aldrich) for 5 h to pre-adsorb the dye onto the catalyst surface. A typical reaction mixture consisted of 10.00 mL of 1.00 mM aqueous rhodamine-6G solution and an appropriate amount of catalyst (e.g., 0.128 g of titania-grafted MCM-41, 0.019 g of anatase, or 0.109 g of MCM-41) in approximately 320 mL of doubly deionized water. The system was air-saturated and stirred at room temperature. The light source was a Pyrex-sheathed 450 W Hanovia brand medium-pressure mercury vapor lamp placed in a water-cooled well in the center of the reactor. Periodically, 10 mL aliquots were removed via a Teflon tube, centrifuged, and analyzed by UV−vis spectroscopy.

α-*Terpineol Oxidation.* A typical reaction mixture consisted of 190 mL of methanol, 10 mL of α-terpineol (Aldrich), and an appropriate amount of catalyst (e.g., 0.133 g of titania-grafted MCM-41, 0.020 g of anatase, or 0.113 g of MCM-41). The reaction mixture was brought to reflux, and 50 mL of 30% H_2O_2 was added. Periodically, 0.5 μL aliquots were removed and injected into a dimethylsilicone capillary GC column with a flame ionization detector.

Results and Discussion

Powder X-ray diffraction (XRD) patterns for the series of MCM-41 and FSM-16 based structures are shown in Figures 1 and 2, respectively. Most of the as-synthesized samples displayed three or four low-angle reflections (d_{100}, d_{110}, d_{200}, d_{210}), which are characteristic of these hexagonal mesostructures (Table 1). The hexagonal order was maintained after calcination of both ungrafted and grafted samples. Singly Ti-grafted MCM-41 or FSM-16 samples (Ti−MCM-41, Ti−FSM-16) did not demonstrate any significant loss of peak intensity for the low-angle reflections. In other reports of the direct incorporation of Ti during the hydrothermal synthesis of mesoporous titanosilicates,[15,23,28−31] the framework order progressively deteriorated with increasing Ti/Si ratio. In fact, no samples with a titanium content greater than 3 wt % have been reported to exhibit strong low-angle peaks in the powder XRD pattern.[23] It is believed that the presence of titanium atoms inside the pore walls introduces defects that can lead to collapse of the framework. In contrast, the current method affixes titania to the surface so that the framework is not weakened by heteroatoms.

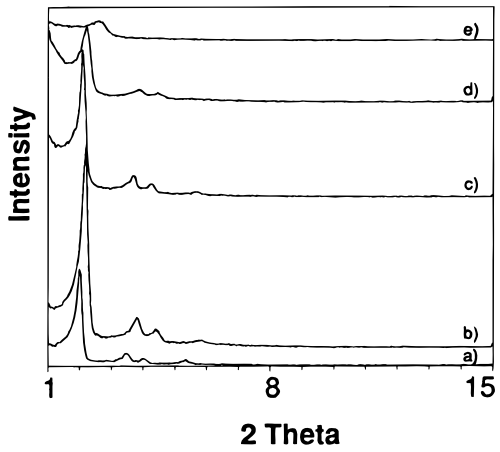

Figure 1. Powder XRD of (a) as-synthesized MCM-41, (b) calcined, ungrafted MCM-41, (c) singly Ti-grafted MCM-41, (d) doubly Ti-grafted MCM-41, grafted in acetone, and (e) doubly Ti-grafted MCM-41, grafted in hexanes.

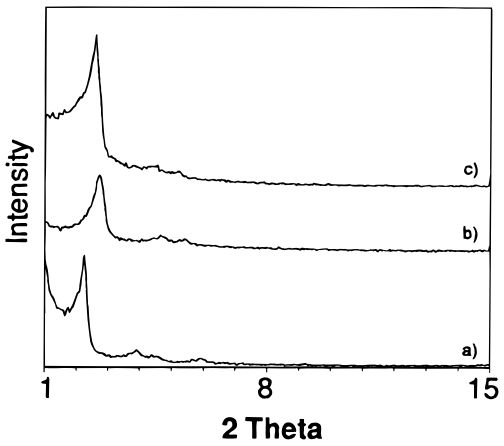

Figure 2. Powder XRD pattern of (a) as-synthesized FSM-16, (b) ungrafted calcined FSM-16, and (c) Ti-grafted FSM-16.

Indeed, the framework appears to be strengthened by addition of titania to the pore surface. After calcination the structure of the nongrafted samples contracted slightly, as indicated by a decrease in the d_{100} spacing. This framework contraction results from further SiO_2 condensation during calcination.[2] Titania-grafted samples experienced a smaller reduction in the d_{100} value upon calcination (see Table 1), which suggests that the titania adds support to the framework, increasing the thermal stability of the structure and preventing some of the framework contraction upon calcination. Such stabilization effects would not be expected from titania particles on the external surface, indicating that at least some of the grafted titania is closely associated with the internal wall structure. The titania could, for example, fill defects in the pore surface that would ordinarily collapse upon calcination. Further evidence for the chemical linkages between titania and the pore surface based on XPS and BET nitrogen adsorption data will be given below.

It should be noted that this grafting technique was initially attempted on calcined (i.e., surfactant-free) mesoporous materials. The XRD patterns of the resulting samples usually showed a complete loss of intensity of the low-angle features after single grafting. Similarly, a large loss of X-ray peak intensity was observed after grafting the calcined Ti−MCM-41 or Ti−FSM-16 with a second titania layer in hexanes (Figure 1e). In

Table 1. Powder XRD Results[a]

sample	*d* spacings (Å)
M8 as-synth	44.1, 27.6, 22.1, 18.0
M8	40.2, 22.9, 19.7, 15.0
TiM8	40.2, 23.0, 19.9
Ti2M8	39.2, 22.6, 19.8, 16.0
M46 as-synth	42.8, 25.2, 23.0, 16.8
M46	34.7, 19.6, 17.6
TiM46a	37.8, 15.3
TiM46b	36.6, 21.9
TiM46c	36.5, 25.6
TiM46d	38.3, 22.0
M79 as-synth	43.9, 25.4, 22.0, 16.6
M79	40.4, 23.2, 20.1, 15.2
TiM79	42.0, 23.9, 20.9, 15.5
M67 as-synth	52.1, 36.1, 29.6, 25.6, 17.8
M67	50.1, 30.5, 25.6, 18.4
TiM67	50.9
M72 as-synth	53.8, 37.0
M72	50.2, 28.2
TiM72	51.7, 32.1
K28 as-synth	35.3, 19.6, 15.5
K28	28.8, 18.5, 15.3, 13.2
TiK28a	32.3, 18.4
TiK28b	32.1
TiK28c	32.1
K43 as-synth	38.1
K43	30.3
TiK43	35.0

[a] Uncalcined samples are labeled "as-synth". All other samples have been calcined. Samples whose label begins with "Ti" are singly Ti-grafted; samples whose label begins with "Ti2" have been doubly grafted. Other numbers are serial numbers referring to the sample of mesoporous material used, while M and K denote MCM-41 or FSM-16, respectively; thus M8 and TiM8 were prepared from the same sample of MCM-41.

these materials, surfactant was absent from the channels and could not prevent large aggregation of titania as $TiCl_4$ hydrolyzed and polymerized. Random clogging of the channels with TiO_2 agglomerates reduced the X-ray order of the mesostructures. When the second grafting was carried out in acetone, only a slight intensity reduction in the low-angle features was observed (Figure 1d). In this case the coordination of acetone molecules with the $TiCl_4$ provided a chemical constraint that prevented excessive polymerization, similar to observations in other reports.[10,12] In any Ti grafting, X-ray absorption by titania may be an additional factor leading to lower peak intensities.

No XRD reflections for bulk anatase were observed for the Ti-grafted mesoporous samples, even after calcination. On the other hand, TEM micrographs (vide infra) showed that some external anatase clusters with ca. 100−250 Å diameters were in fact present on some samples. Since particles of these dimensions should still be observable by XRD, the absence of any corresponding diffraction lines in these samples suggests that their concentration was relatively low. In comparison, a reference sample of Ti-grafted *nonporous* silica particles exhibited an XRD reflection at $d = 3.53$ Å, which corresponds to the (101) reflection for anatase, the most intense feature in the anatase powder XRD. A sample of bulk titania prepared from $TiCl_4$ was X-ray amorphous before calcination; after calcination, an XRD pattern characteristic of anatase was observed.

The TEM image and selected-area diffraction pattern (Figure 3) show the hexagonally ordered mesostructure of the MCM-41 support, unaffected by the presence of titania in this sample. The evolution of potentially

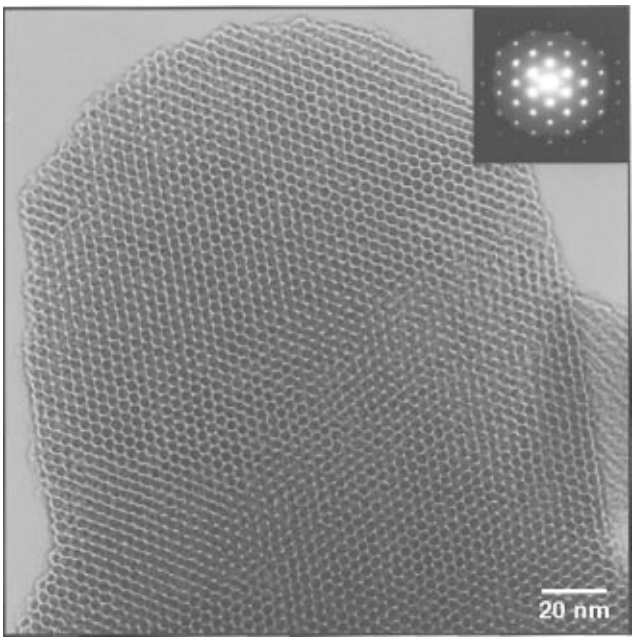

Figure 3. TEM image of a singly Ti-grafted MCM-41 particle. Inset: selected-area diffraction pattern of this particle.

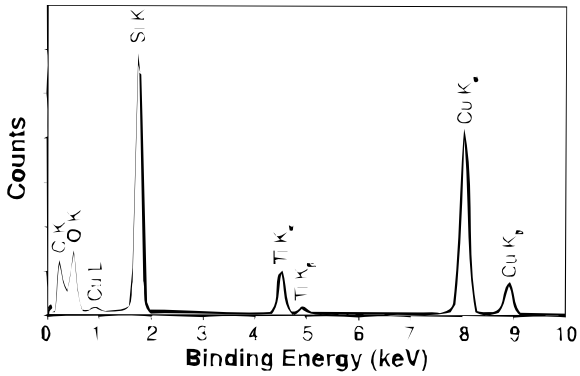

Figure 4. TEM-EDS spectrum of the region of singly Ti-grafted MCM-41 shown in Figure 3. The carbon and copper peaks arise from the support grid.

damaging HCl in the grafting procedure has been cited as a concern with using $TiCl_4$ as the titanium source;[10] however, as can be seen in Figure 3, the grafting technique does not cause significant deterioration of the silica framework. Additionally, no titania clusters can be seen, indicating that any clusters or layers formed by the titania must be very small. However, TEM images of some grafted samples have shown the presence of a small fraction of external 100−250 Å crystallites. A selected-area diffraction pattern and an X-ray energy-dispersive spectrum of these particles reveals that they are composed of anatase, a polymorph of TiO_2.

EDS analysis was carried out both on the TEM and SEM instruments. EDS performed on the mesoporous region shown in Figure 3 (i.e., where no anatase crystallites are visible) produced a strong Ti signal with an approximate Si:Ti ratio of 8.7:1 (Figure 4), slightly larger than that obtained from chemical elemental analysis of the bulk sample (Table 2). EDS elemental maps obtained on the SEM for a singly grafted MCM-41 particle are shown in Figure 5. The image formed from the titanium signal matches that of the silicon signal, though the former is somewhat lower in intensity. Comparison of parts b and c in Figure 5 shows that titania is present in all areas where silica is

Table 2. Comparative Table of Results from UV−Vis Spectroscopy and Elemental Analysis[a]

sample	band edge (nm)	wt % of Titanium	Si:Ti mole ratios
TiM8 (24 h)	356 (±3)	9.33	6.38
Ti2M8 (24 h)	363 (±1)	9.48	6.22
TiM53 (4 h)	349 (±1)	3.76	15.9
Ti2M53 (4 h)	358 (±2)	9.09	6.16
TiM67 (5.5 h)	355 (±3)	9.69	5.74
TiM72 (24 h)	355 (±2)	8.46	6.88
TiK28a (4 h)	352 (±4)	5.27	9.10
TiK43 (4.5 h)	355 (±2)	6.10	10.7

[a] Sample notation is the same as that in Table 1. The time of sample exposure to the $TiCl_4$ solution is given in parentheses.

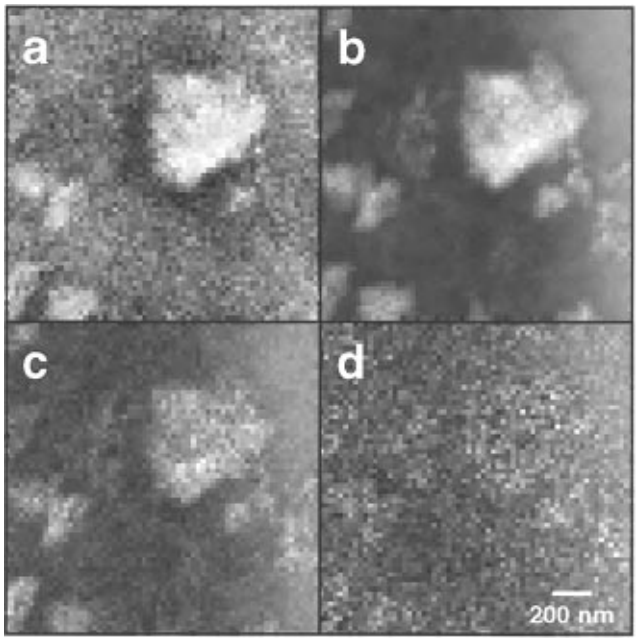

Figure 5. (a) Backscattered electron image of the singly Ti-grafted MCM-41 particle used to produce the EDS elemental maps generated by the signal from (b) silicon and (c) titanium. (d) Background image.

present, establishing that the titania is evenly dispersed throughout the system.

To determine whether Si−O−Ti bonds had formed in the grafting process, IR and XPS measurements were performed. IR studies showed a peak at 960 cm^{-1} that increased in intensity for higher titania loadings. The 960 cm^{-1} peak is commonly attributed to the Si−O stretching vibration of a polarized $Si-O^{\delta-}- - -Ti^{\delta+}$ bond.[32,33] The XPS results for the singly grafted sample TiM8 are summarized in Table 3. The assignments are based on published binding energy (BE) shifts for SiO_2,[34,35] TiO_2,[36] and SiO_2/TiO_2[35,37] mixed oxide systems.

Table 3. Binding Energies and Atomic Concentrations Observed from the X-ray Photoelectron Spectra of TiM8

element/orbital	binding energy (eV)	atomic concn (%)	assignment
Si 2p	103.8	25.59	SiO_2 (C. N. 4)
O 1s	535.0	2.88	Si−OH
	533.2	50.97	SiO_2, H_2O,(bridged TiOH)
	531.6	6.49	Si−O−Ti, (terminal TiOH)
	530.1	3.30	TiO_2
Ti $2p_{3/2}$/Ti $2p_{1/2}$	460.3/466.0	0.94	Ti−O−Si
	458.8/464.5	1.63	TiO_2 (anatase)
	456.8/462.5	0.10	TiO?

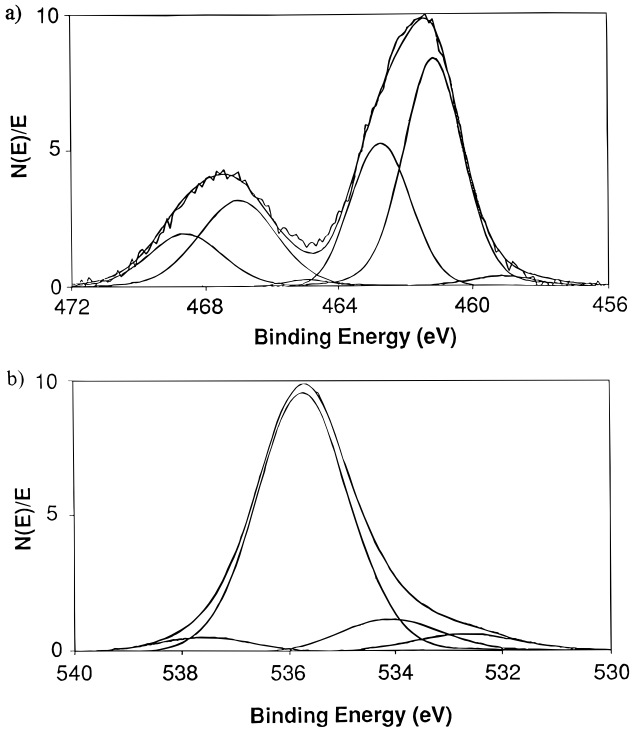

Figure 6. XPS spectra of singly Ti-grafted MCM-41, focusing on (a) the Ti $2p_{3/2}$ peak and (b) the O 1s peak. The smooth curves are computer-simulated curves obtained in the curve-fitting routine; the lower intensity smooth curves are the individual deconvoluted peaks.

Figure 6a shows the XPS spectrum in the Ti $2p_{1/2}$/Ti $2p_{3/2}$ binding energy region. A distinct asymmetry can be observed in both peaks, indicating the presence of more than one environment for titanium atoms. Curve fitting was possible with two components for each peak (460.3/466.0 eV and 458.8/464.5 eV) but was improved by including a small fraction of a third component at 456.8/462.5 eV. The largest central peak (at 458.8/464.5 eV) is consistent with titanium in the octahedral hcp environment of anatase and probably originates from the large (ca. 100 Å diameter) anatase particles that are present on the external surface of some particles. Titania present within the channels will also contribute to this XPS peak if the local environment is similar to anatase. The BE of the second largest contribution (460.3/466.0 eV), ca. 35 atomic % of the total TiO_2, coincides with that for titania closely associated with silica, where cross-linking Ti−O−Si bonds act as bridges between TiO_2 and SiO_2 moieties, consistent with the IR

(28) Alba, M. D.; Luan, Z.; Klinowski, J. *J. Phys. Chem.* **1996**, *100*, 2178.
(29) Franke, O.; Rathousky, J.; Schultz-Ekloff, G.; Stárek, J.; Zukal, A. *Stud. Surf. Sci. Catal.* **1994**, *84*, 77.
(30) Corma, A.; Navarro, M. T.; Pérez-Pariente, J.; Sánchez, F. *Stud. Surf. Sci. Catal.* **1994**, *84*, 69.
(31) Morey, M.; Davidson, A.; Stucky, G. D. *Micropor. Mater.* **1996**, *6*, 99.
(32) Boccuti, M. R.; Rao, K. M.; Zecchina, A.; Leofanti, G.; Petrini, G. *Stud. Surf. Sci. Catal.* **1984**, *48*, 133−144.
(33) Crocker, M.; Emeis, K. A.; Herold, R. H. M. *J. Mol. Catal. A* **1996**, *110*, L7−L11.
(34) Wagner, C. D.; Zatko, D. A.; Raymond, R. H. *Anal. Chem.* **1980**, *52*, 1445−1451.
(35) Stakheev, A. Y.; Shpiro, E. S.; Apijok, J. *J. Phys. Chem.* **1993**, *97*, 5668−5672.
(36) Murata, M.; Wakino, K.; Ikeda, S. *J. Electron Spectrosc. Relat. Phenom.* **1975**, *6*, 459−464.
(37) Fernandez, A.; Leyrer, J.; Gonzáles-Elipe, A. R.; Munuera, G.; Knözinger, H. *J. Catal.* **1988**, *112*, 489−494.

spectra.[35,38,39] Additionally, the Si 2p BE for the titania-grafted MCM-41 sample is shifted to a value (103.8 eV) that is identical with the BE observed for a 15 wt % TiO_2/SiO_2 mixed oxide structure; the BE of silica usually decreases upon substitution of the Si atoms by less electronegative, more polarizable Ti atoms.[35] Finally, the third component of the Ti $2p_{1/2}$/Ti $2p_{3/2}$ peaks matches the BE of a cubic TiO sample with a NaCl structure (octahedral Ti) and a long Ti−O bond length of 2.09 Å.[40]

The O 1s XPS peak is too broad and asymmetric for a single band (Figure 6b); the best fit was achieved using four component peaks. A contribution from oxygen in silanol groups (535.0 eV) is observed in addition to oxygen in Si−O−Si and Ti−O−Ti bonds (533.2 and 530.1 eV, respectively). Furthermore, a peak at an intermediate BE value of 531.6 eV is clearly present, which is assigned to oxygen in interfacial Si−O−Ti cross-linking bonds.[35,38,39] The shift of this peak from the titania peak has been ascribed to a decrease in the negative charge of the oxygen as well as in the polarizability, which leads to a decrease in the ionic character of the bonds connecting the silica and titania phases, compared to bulk titania.[39] The presence of the peak at 531.6 eV further supports the conclusion that titania is chemically bound to the MCM-41 channel walls. The binding energies for bridged and terminal hydroxyl groups on titanium (533.7 and 532.5 eV, respectively)[41] overlap with the region for SiO_2 and Si−O−Ti oxygens. These were not resolved separately.

Further information regarding the form and location of grafted titania was gained from nitrogen adsorption, UV−vis and ^{1}H NMR spectroscopies, as well as from a small-angle neutron diffraction experiment. Nitrogen adsorption experiments and BET calculations of the grafted samples and ungrafted, calcined samples provided insight on the pore shape and surface area of the system. The mesoporous materials exhibited type IV isotherms with narrow hysteresis loops (Figure 7), characteristic of mesoporous materials with pore diameters in the range 20−40 Å.[42] Hysteresis loops for ungrafted, calcined samples appeared to be composites of type H1 and H4 models. Type H1 hysteresis, in which the loop appears on the vertical portion of the type IV isotherm, is usually produced for mesoporous materials with cylindrical pores. On the other hand, type H4 hysteresis, in which the loop is seen on the horizontal portion of the isotherm and little of the vertical portion is detected, is believed to represent slit-shaped pores with some microporosity (pore diameters $<\sim$20 Å).[8] Combination H1/H4 hysteresis loops, typical for MCM-41 at the lower end of the mesoporous range, can be attributed to cylindrical pores that are sufficiently narrow that the N_2 adsorbate begins to have difficulty forming a typical meniscus, leading to the semblance of microporosity.[42] Hysteresis loops for the grafted samples were similar in shape to those of ungrafted samples, suggesting a regular dispersion of

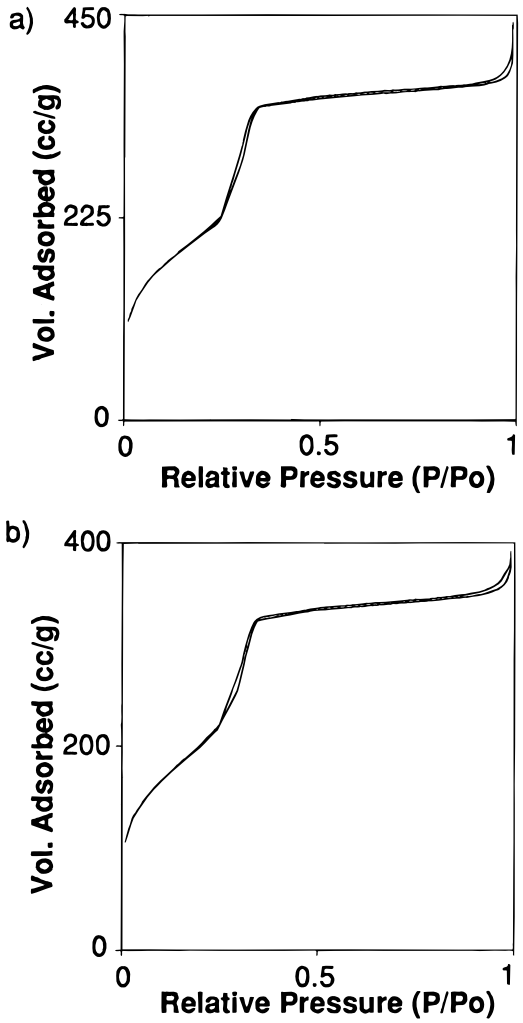

Figure 7. N_2 adsorption isotherms of (a) ungrafted calcined MCM-41 and (b) Ti-grafted MCM-41.

TiO_2 throughout the pores. Importantly, the broad, almost square-shaped loop indicative of a type H2 hysteresis loop was not observed in most of the isotherms. Although the interpretation of the type H2 hysteresis loop has been the subject of some debate, it is commonly associated with "ink bottle" shaped pores, in which the area near the opening is narrower than the main body of the pore.[8] Had the TiO_2 formed primarily at the opening of the channel, rather than diffusing through the entire pore, the isotherm would have exhibited more H2 character.

Table 4 lists the changes in saturation pressure, surface area, and pore volume for several representative samples. Although the grafted samples were not prepared directly from the ungrafted samples listed (see Experimental Section), small but repeatable decreases in saturation pressure, surface area, and pore volume were usually observed. The systematic drops in saturation pressure and, more importantly, pore volume indicate that titania is grafted onto the pore surface. The saturation pressure is indicative of the amount of N_2 required to completely fill all the pores in the system. If the titania is grafted in the pores, as suggested by the decrease in pore volume, the amount of N_2 needed to completely fill the pores decreases, thus lowering the saturation pressure.[43] Because narrowing of the pores is the only explanation for the decrease in pore volumes

(38) Ingo, G. M.; Dirè, S.; Babonneau, F. *Appl. Surf. Sci.* **1993**, *70/71*, 230−234.
(39) Lassaletta, G.; Fernández, A.; Espinós, J. P.; González-Elipe, A. R. *J. Phys. Chem.* **1995**, *99*, 1484−1490.
(40) Liu, Z.; Davis, R. J. *J. Phys. Chem.* **1994**, *98*, 1253−1261.
(41) Metson, J. B.; Hyland, M. M.; Gillespie, A.; Hemmingsen-Jensen, M. *Colloids Surf. A: Physicochem. Eng. Aspects* **1994**, *93*, 173−180.
(42) Llewellyn, P. L.; Grillet, Y.; Schüth, F.; Reichert, H.; Unger, K. K. *Micropor. Mater.* **1994**, *3*, 345.
(43) Wu, C. G.; Bein, T. *Science* **1994**, *264*, 1757.

Table 4. Representative Results of N_2 Adsorption Experiments, Based on BET Calculations[a]

sample	saturation pressure (mmHg)	surface area (m^2/g)	pore vol (cm^3/g)	av pore diam (Å)	peak pore diameter
M6	761	1089	0.697	25.6	21
TiM6b	760	1018	0.615	24.2	21
Ti2M6a	759	806	0.503	25	21
M8	773	750	0.683	36.4	26
TiM8	774	725	0.605	33.4	26
Ti2M8	770	683	0.624	36.5	25
M79	751	918	0.795	34.6	27
TiM79	747	758	0.682	34.7	27

[a] All samples were calcined prior to analysis. Sample labeling is the same as that described for Table 1. The average pore diameter is calculated from the surface area and pore volume. The peak pore diameter corresponds to the peak in the adsorption pore size distribution plot.

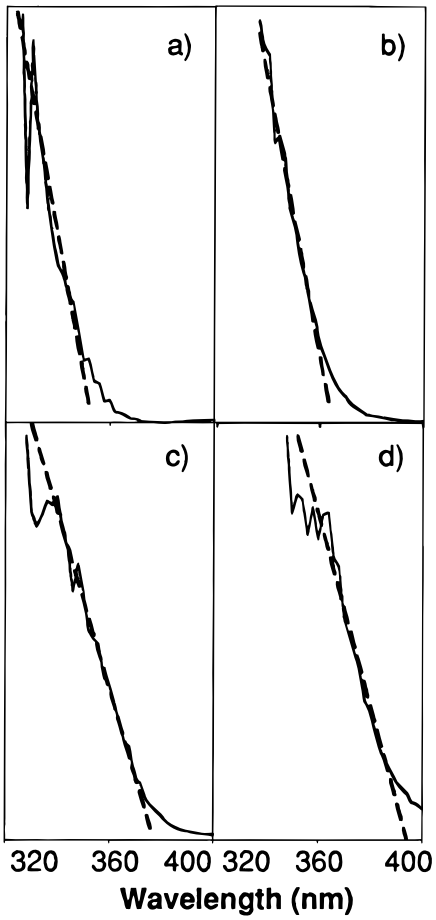

Figure 8. Diffuse reflectance UV−vis spectra of (a) singly Ti-grafted MCM-41 (band edge = 355 nm), (b) twice Ti-grafted MCM-41 (band edge = 365 nm), (c) titania grafted onto nonporous silica (band edge = 377 nm), and (d) bulk anatase titania (band edge = 393 nm). Band edges are extrapolated.

and saturation pressures, it is logical to conclude that the titania is deposited inside the pores.

Figure 8 shows the diffuse reflectance UV−vis spectra (corrected using the Kubelka−Munk equation) of the band edges of singly grafted and doubly grafted MCM-41, Ti-grafted nonporous silica, and bulk anatase. A band edge of 352−356 nm is observed for a singly Ti-grafted sample, a significant blue shift from the band edge of 393 nm for calcined bulk titania (anatase). The blue shift is caused by quantum size effects that are observed in semiconductors as the particle size decreases. In titania, a large-bandgap semiconductor, particle sizes below 50 Å in diameter are sufficient to induce the optical confinement effects that generate the increased bandgap energy.[44] Therefore, in Ti−MCM-41 the titania must be present as particles significantly smaller than 50 Å. The blue shift diminished with increased titania loading, implying an increase in titania particle size. In all samples exhibiting a band edge of less than 370 nm, no bulk titania features were noted in the powder XRD patterns. However, samples with a band edge of 370 nm or higher, such as the grafted nonporous silica sample or samples prematurely exposed to air or water, showed some bulk anatase features in the XRD pattern.

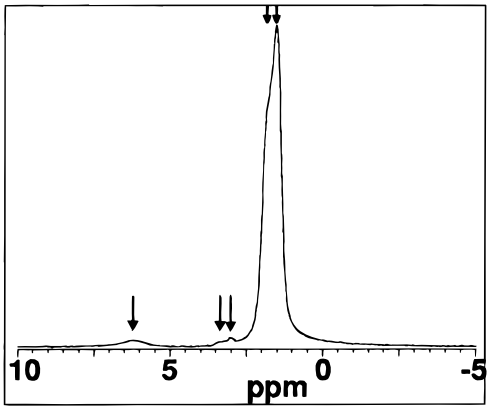

Figure 9. Solid-state ^{1}H MAS NMR spectrum of singly Ti-grafted MCM-41.

The blue shift, or increased bandgap energy, can be used to estimate the size of the semiconductor particles. The bandgap shift is given by[44]

$$\Delta E_g = (h^2\mu/8R^2) - (1.8e^2/\epsilon R) \quad (1)$$

where μ is the reduced effective mass ($1/\mu = 1/m^*_e + 1/m^*_h$) of the electron and hole, R is the particle radius, e is the elementary charge, and ϵ is the dielectric constant of the semiconductor.[44] Values in the ranges, $0.01-3m_e$, $5-30m_e$, and $14-184$ have been reported for the effective mass of the hole, effective mass of the electron, and dielectric constant of titania, respectively.[39,44,45] Kormann's values for the effective reduced masses ($m^*_e = 9m_e$ and $m^*_h = 2m_e$) were used in the determination of the particle size in the present study.[44] By using the entire range of dielectric constants, one can estimate titania cluster diameters of 12−16 Å for a corresponding UV−vis band edge of 355 nm. Assuming spherical particles and an anatase unit cell, such clusters would contain approximately 30−70 TiO_2 units each.

Solid-state ^{1}H MAS NMR has been established as a useful technique for determining the configuration of TiO_2 particles too small to be detected by powder XRD by examining the chemical shifts of the TiOH protons.[46] The solid-state ^{1}H MAS NMR spectrum of a singly Ti-grafted sample of MCM-41 (Figure 9) displayed resonances at 6.2, 3.4, 3.0, 1.8 (shoulder), and 1.5 ppm. In previous work by Crocker,[46] the anchoring of titania onto silica (via a reaction of $Ti(CH_2C_6H_5)_4$ with silica

(44) Kormann, C.; Bahnemann, D. W.; Hoffman, M. R. *J. Phys. Chem.* **1988**, *92*, 5196.
(45) *CRC Handbook of Chemistry and Physics*, 70th ed.; Weast, R. C., Lide, D. R., Astle, M. J., Beyer, W. H., Eds.; CRC Press: Boca Raton, FL, 1989.
(46) Crocker, M.; Herold, R. H. M.; Wilson, A. E.; Mackay, M.; Emeis, C. A.; Hoodendorn, A. M. *J. Chem. Soc., Faraday Trans.* **1996**, *92*, 2791.

gel, followed by calcination) resulted in peaks at 6.3 and 3.4−3.2 ppm; the former peak was characteristic of anatase, which had not been observed in the XRD pattern. The latter feature was determined to be indicative of tetrahedrally coordinated titanium, though it was not possible to resolve single (TiOH) or geminal ($Ti(OH)_2$) hydroxyl peaks.[46] In the same report, isolated peaks at $\delta < 2.0$ ppm were attributed to terminal silanol peaks (the difference in chemical shift between single and geminal silanol groups was less than 0.1 ppm and too small to be resolved). Accordingly, in the ^1H MAS NMR spectrum of singly grafted MCM-41, the resonance at 6.2 ppm can be assigned to the bridging TiOH protons in an anatase-like environment; the peak at 3.0 ppm is probably due to hydrogen-bonded terminal TiOH protons. An anatase configuration is not surprising, as amorphous titania calcined at 550 °C is transformed into anatase rather than other polymorphs. The peak at 3.4 ppm occurs at a chemical shift for TiOH in a tetrahedral coordination about the titanium center. The peak at 1.5 ppm can be attributed to terminal silanols on the pore surface, while the shoulder at 1.8 ppm is probably due to a fraction of terminal silanols hydrogen bonded to terminal titanium hydroxide groups. The intensity of the SiOH peak indicates that many of the available surface hydroxides have not reacted with the $TiCl_4$ and that the channel walls are not completely covered with a smooth titania layer. The chemical shifts of the titania peaks suggest that the titanium atoms are present in two types of environment, a tetrahedrally coordinated phase and an anatase-like phase, while the comparatively low intensity of these peaks indicates that few hydroxides are present in the titania phases.

Neutron-scattering density contrast matching experiments were performed using small angle neutron scattering (SANS). The intensity distribution $I(q)$ for small-angle scattering can be analyzed by using the Guinier approximation, which is described by

$$I(q) = NV^2(\Delta\rho)^2\exp(-q^2R_g{}^2/3) \qquad (2)$$

where N is the number of particles, V the particle volume, $(\Delta\rho)$ the difference in the scattering length density of the particle and any solvent present, R_g the radius of gyration, and q the wave vector (which is related to the d spacing via $q = 2\pi/d$).[47] The variation of the intensity with the scattering angle in the small-angle scattering region (Guinier region) can be described by various power laws, with exponents that are characteristic for a given geometry. Figure 10a shows a log I vs log q SANS plot for singly Ti-grafted MCM-41. The peak at $q = 0.14$ Å^{-1} corresponds to the d_{100} reflection from the XRD pattern, while the slope in the linear portion of the $q < 0.08$ Å^{-1} region is characteristic of the semicrystalline structure of MCM-41. It is possible to select either the titania or the silica portion of the structure by filling the pores with a contrast-matching fluid.[48−50] Figure 10b shows the SANS pattern for the same singly grafted MCM-41 sample when it is saturated with a 66% D_2O/34% H_2O solution. Because the neutron-scattering density for this solution matches that of silica, the silica signal is nullified in the SANS pattern and only the diffraction due to titania is observed. As shown in Figure 10b, the peak at $q = 0.14$ Å^{-1} disappears, which would appear to be inconsistent with other analyses that show the titania to be thoroughly dispersed throughout the system. However, particles smaller than roughly 10 Å cannot be observed by this technique, so the dispersed titania observed by EDS must be in the form of very small particles, in agreement with the UV−vis data. Additionally, the $q < 0.08$ Å^{-1} region exhibits a linear portion, the slope of which corresponds to particles with a radius of gyration of 100 ± 20 Å, consistent with the external particles observed by TEM in this sample.

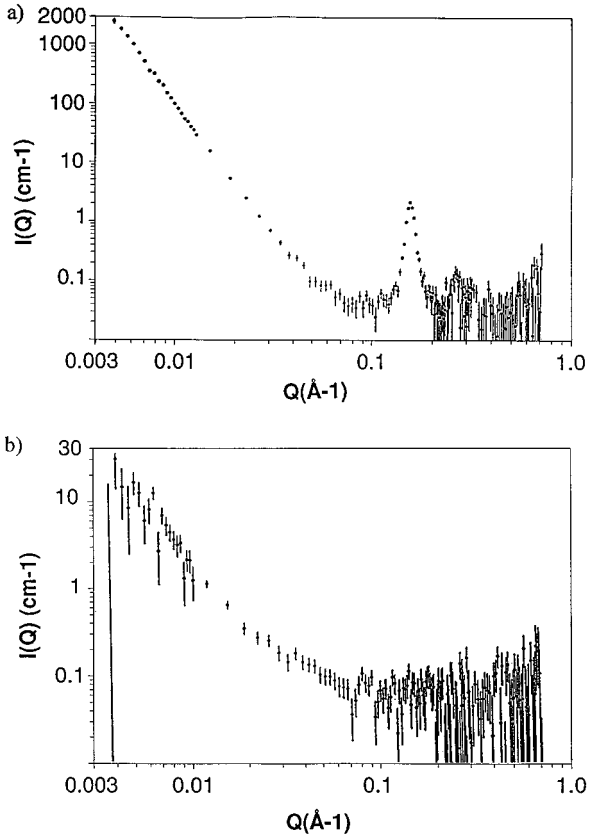

Figure 10. log I vs log q SANS plots for (a) singly Ti-grafted MCM-41 and (b) singly Ti-grafted MCM-41 in 66%D_2O/33%H_2O solution.

Figure 11 outlines the reaction scheme and models of potential structures resulting from the grafting procedure. On the basis of the observed color changes, analytical evidence, and published reports,[51] it is believed that the $TiCl_4$ diffuses through the nonpolar hydrocarbon tails of the surfactant that fills the pores. The $TiCl_4$ then moves to the polar head of the surfactant, forming a bright yellow chloride/amine complex. A similar color change was noted by Maschmeyer et al. in a report describing the reaction of titanocene dichloride with calcined MCM-41.[10] The physical constraint of the pore walls and the chemical constraint of the surfactant act as barriers to the formation of large titania agglomerates. Titania becomes anchored to the silica framework via reaction with terminal SiOH

(47) Carrado, K. A.; Thiyagarajan, P.; Winans, R. E.; Botto, R. E. *Inorg. Chem.* **1991**, *30*, 794−799.
(48) Bradley, K. F.; Chen, S. H.; Thiyagarajan, P. *Phys. Rev. A* **1990**, *42*, 6015−6023.
(49) Glinka, C. J.; Nicol, J. M.; Stucky, G. D.; Ramli, E.; Margolese, D.; Huo, Q.; Higgins, J. B.; Leonowicz, M. E. *J. Porous Mater.* **1996**, *3*, 93−98.
(50) Bendedouch, D.; Chen, S.-H.; Koehler, W. C. *J. Phys. Chem.* **1983**, *87*, 153−159.
(51) Kim, A. Y.; Lui, J.; Virden, J. W.; Bunker, B. *Mater. Res. Soc. Symp. Proc.* **1995**, *371*, 105.

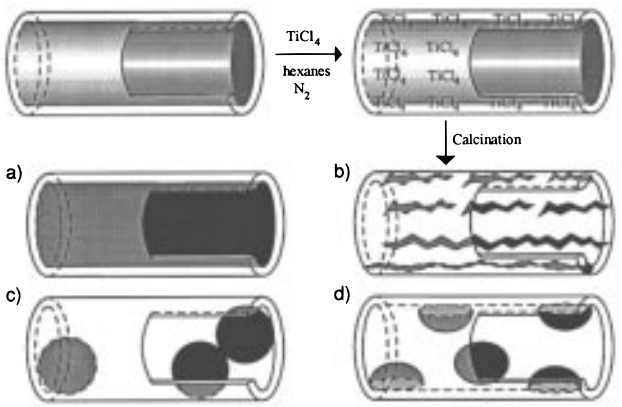

Figure 11. Schematic of the grafting procedure and potential results. A single pore is shown. The white region represents the silica framework, the black represents titania, and the gray gradient represents the surfactant. A sample of as-synthesized MCM-41 or FSM-16 is exposed to a solution of $TiCl_4$ in hexanes under N_2 for 24 h. The sample is then rinsed with hexanes, dried, and calcined. (a) A smooth layer of TiO_2 coats the pore surface. (b) TiO_2 forms in irregularities in the pore surface, as either nanoclusters or isolated TiOH. (c) TiO_2 forms irregularly distributed agglomerates inside the pores. (d) TiO_2 forms slightly flattened hemispheres that are fairly evenly dispersed throughout the system. The model in (d) most closely fits the evidence to date.

groups on the pore surface. Several models can be proposed for the form that the titania takes upon hydrolysis. The model of titania forming a smooth layer that completely coats the pore surface is ruled out by the ^1H NMR and XPS results. Instead, the $TiCl_4$ could settle in irregular or systematic defects in the pore surface, forming $(TiO_2)_n$ nanoclusters or isolated TiO_2 units that smooth the pore surface. It is possible that the titania could form as irregularly distributed agglomerates that partially or completely block many of the pores; however, this model has been ruled out by XRD and N_2 adsorption. Finally, the titania could be described as nanoclusters that are well dispersed throughout the system.

To elucidate the shape of the titania particles within the pores, some approximate calculations were made. The external surface area of 0.1−1 μm particles amounts to only ca. 0.2−2% of the surface area measured for the Ti−MCM-41 samples. From the XPS data, it can be shown that the fraction of the surface covered by titania (coverage = %Ti−O−Si/(%Ti−O−Si + %Si−OH)) is approximately 14% and that roughly one-third of the Ti atoms are involved in Si−O−Ti bonds. By estimating the surface area of 100 Å particles to be 153 m^2/g (from the sphere volume and the density of anatase) and treating the total surface area of a grafted sample as a weighted average of the crystallites and nongrafted MCM-41, it can be shown that, at most, only 25% of the titania added to the system can be present as external crystallites. The other 75% of the titania must be located inside the pores. From the percent coverage and the change in pore volumes, a particle thickness of about 10 Å can be estimated, which, when combined with the 14% coverage obtained from the XPS, suggests the titania particles are shaped like slightly flattened spheres or hemispheres with approximate diameters of 11−17 Å.

The hemisphere titania particle model fits well with the evidence gathered to date. The particles are too minute and too dispersed to be observable by SANS and TEM (and unresolvable by the SEM elemental maps) while being sufficiently small to display the blue shift in the UV−vis. The dispersion would also lead to little change in the N_2 adsorption isotherm and XRD pattern; the slight change in the d_{100} reflection could indicate that some particles anchor in a defect in the pore wall, filling it and preventing its collapse upon calcination. The UV−vis data indicate an increase in the titania particle size upon the second grafting step. Growth can occur at silanol sites around the existing particles. XPS and NMR results show that a significant number of silanol sites are available near the titania agglomerates for additional reaction with $TiCl_4$. Band-edge calculations imply that a change in particle radius of up to 1 Å is sufficient to red shift the band edge by 8 nm, which would explain why the second grafting carried out in acetone has a dramatic effect on the band edge but not on the titanium content of the sample (Tables 1 and 2, sample Ti2M8).

The catalytic activity of the titania-grafted MCM-41 samples was tested using the photobleaching reaction of rhodamine-6G (R-6G) and the oxidation reaction of α-terpineol. R-6G has a relatively high resistance to photo- and oxidative degradation and has been used as a model compound for solar detoxification of wastewaters containing dyes, nitrate esters, or other toxic organic chemicals.[52,53] The oxidative decomposition of R-6G is catalyzed by $Ti^{IV}-OH^{\bullet}$ surface hydroxyl radicals, which are generated in an aqueous environment after photoexcitation of TiO_2 at wavelengths < 388 nm.[54] A plot of the relative absorbance of an R-6G dye solution vs time of UV irradiation (Figure 12a) shows a large increase in conversion for Ti−MCM-41 samples (ca. 9 wt % Ti) compared to uncatalyzed reactions or reactions catalyzed by anatase. Table 5 lists the corresponding 1-h conversions and pseudo-first-order rate constants.[55] The average values for both percent conversion and rate constant are ca. 5 times larger than for anatase but smaller than for P25 TiO_2. The rate constants are comparable to those obtained with amorphous TiO_2/SiO_2 catalysts of similar composition, prepared by sol−gel synthesis.[53] The photocatalytic activity of Ti−MCM-41 did not change significantly after limited repeated use.

α-Terpineol has previously been used as a large test molecule to study the intrinsic activity of directly synthesized Ti−MCM-41 (ca. 2 wt % TiO_2).[15,30] In the present study the catalyzed oxidation of α-terpineol was carried out under similar conditions. Results are shown in Figure 12b and Table 6. Ungrafted MCM-41 exhibited no catalytic activity. The Ti-grafted MCM-41 samples again resulted in a great increase in percent conversion and reaction rate compared to anatase, as well as P25 TiO_2. The conversions were a significant improvement over those observed for directly synthesized Ti−MCM-41 (27.8% after 3 h[30] and 44.6% after 9 h[15]). However, as expected for a distribution of small

(52) Muradov, N. Z. *Solar Energy* **1994**, *52*, 283−288.
(53) Anderson, C.; Bard, A. J. *J. Phys. Chem.* **1995**, *99*, 9882−9885.
(54) Mills, A.; Belghazi, A.; Davies, R. H.; Worsley, D.; Morris, S. *J. Photochem. Photobiol. A: Chem.* **1994**, *79*, 131−139.
(55) The photobleaching of R-6G has usually been treated as a first-order reaction.[53,54] If Knudsen flow is assumed for the dye molecules and their decomposition products in the mesopore channels, a pseudo-first-order reaction should still be observed. Wheeler, A. *Adv. Catal.* **1951**, *3*, 249−326.

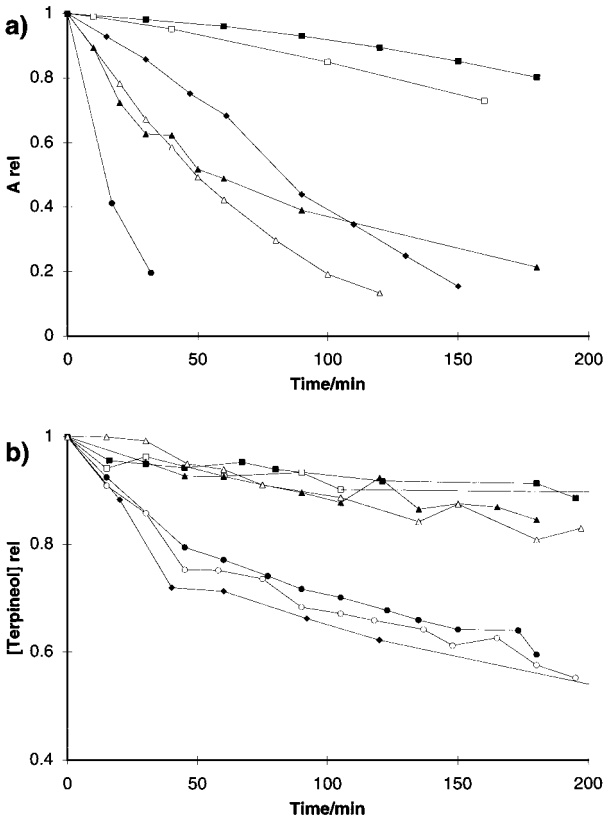

Figure 12. (a) Plot of A_{rel} (absorbance/initial absorbance) at λ = 526 nm vs irradiation time for the photobleaching of rhodamine-6G, sensitized by various catalysts: (■) no catalyst added; (□) anatase; (◆, △, ▲) Ti−MCM-41 samples (ca. 9 wt % Ti); (●) P25 TiO_2. (b) Plot of relative α-terpineol concentration (relative GC peak area due to α-terpineol) vs time for the oxidation reaction with H_2O_2 and various catalysts: (□) no catalyst added; (■) MCM-41; (▲) anatase; (△) P25 TiO_2; (●, ○, ◆) Ti−MCM-41 samples (ca. 9 wt % Ti). (○) and (●) were obtained sequentially with the same catalyst sample.

Table 5. Activity of Ti−MCM-41 for Rhodamine-6G Photodegradation

sample	% conversion (60 min)	k[a] (h^{-1})
no catalyst	4.1	0.10
anatase	10.4	0.15
Ti−MCM-41[b]	50.4	0.78
P25 TiO_2	100.0	3.06

[a] Pseudo-first-order reaction rate. [b] Average of four reactions.

Table 6. Activity of Ti−MCM-41 for α-Terpineol Oxidation

sample	% conversion (60 min/180 min)	k[a] (h^{-1})
no catalyst	5.7/10.8	0.03
MCM−41	5.0/8.6	0.02
anatase	7.3/15.4	0.04
P25 TiO_2	6.0/19.1	0.05
Ti-MCM-41[b]	25.4/42.3	0.16

[a] Pseudo-first-order reaction rate. [b] Average of three reactions.

titania agglomerates within the MCM-41 channels, the product selectivity was very low in the grafted samples. It has been suggested that water present in the reaction coordinates with titanium, lowering both the reactivity and selectivity of the catalyst.[15] With their high catalytic activity but low product selectivity, these high surface area mesoporous materials may be most suitable for the decomposition of pollutants rather than for fine chemical synthesis.

Conclusion

This study has demonstrated that $TiCl_4$ is a viable precursor for grafting titania onto the internal surface of mesoporous supports. The presence of surfactant in the channels prevents large particle agglomeration. The surfactant constrains the $TiCl_4$, limiting its predilection toward rapid polymerization and enabling it to form small flattened titania hemispheres on the pore surface. IR and XPS confirm the formation of Ti−O−Si, while powder XRD, TEM, and EDS indicate that the titania is well dispersed throughout the system. N_2 adsorption experiments corroborate the conclusion that titania is present on the pore surface, and powder XRD indicates that the grafting procedure helps strengthen the mesoporous framework. Finally, the SANS scattering density matching and diffuse reflectance UV−vis experiments show that titania is present as minute clusters containing ∼30−70 TiO_2/cluster. Additional grafting steps enable manipulation of the bandgap of the grafted titania, permitting tunability of titania's optical properties through quantum size effects.

This method provides an alternative to the direct synthesis of titanosilicate mesoporous sieves and to grafting methods with titanocene dichloride or similar organotitanium precursors.[10] The products of the new technique can be advantageous in certain circumstances. The direct synthesis is the simplest method allowing titanium incorporation into the framework. However, only low titanium loadings have so far been possible or products with low order were obtained. Grafting with titanocene dichloride can be carried out on highly ordered supports; it produces isolated oxotitanium sites on the pore surface. When aggregates of adjacent titanium oxide sites are required for certain photooxidation reactions, the grafting method with less expensive $TiCl_4$ in the presence of the surfactant yields titania nanoclusters well dispersed over the internal pore surface of the mesoporous support. High loadings (exceeding 9 wt % titanium) are possible, and the large surface area and structural order can be maintained.

Acknowledgment. A.S. acknowledges 3M, the David and Lucille Packard Foundation, the donors of the Petroleum Research Fund, administered by the American Chemical Society, and the Office of the Vice President for Research and Dean of the Graduate School of the University of Minnesota for support of this research. This work has benefitted from the use of the Intense Pulsed Neutron Source at Argonne National Laboratory. This facility is funded by the U.S. Department of Energy, BES-Materials Science, under Contract W-31-109-Eng-38. The authors acknowledge the assistance of P. Thiyagarajan (IPNS) and B. T. Holland (University of Minnesota) with the SANS experiment, A. Wright (Surface Analysis Center, University of Minnesota, XPS analysis), S. McKernan (Center for Interfacial Engineering at the University of Minnesota, electron microscopy), and P. Isbester (University of Minnesota, solid-state NMR). We thank Professor C. B. Carter (Chemical Engineering and Materials Science) for helpful discussions regarding the microscopy work. C.F.B. gratefully acknowledges the Center for Interfacial Engineering at the University of Minnesota for a CIE-NSF graduate fellowship.

CM970180K